

Simulation of statistically accurate time-integrated dynamic speckle patterns in biomedical optics

EDWARD JAMES^{1,*}, SAMUEL POWELL^{1,2}, AND PETER MUNRO¹

¹Department of Medical Physics & Biomedical Engineering, University College London, London, WC1E 6BT, UK

²Faculty of Engineering, The University of Nottingham, University Park, Nottingham, NG7 2RD, UK

*Corresponding author: e.james.14@ucl.ac.uk

Compiled August 5, 2021

The simulation of statistically accurate time-integrated dynamic speckle patterns using a physics-based model that accounts for spatially varying sample properties is yet to be presented in biomedical optics. In this letter we propose a solution to this important problem based on the Karhunen-Loève expansion of the electric field, and apply our method to the formalisms of both laser speckle contrast imaging and diffuse correlation spectroscopy. We validate our technique against solutions for speckle contrast for different forms of homogeneous field, and also show that our method can readily be extended to cases with spatially varying sample properties. © 2021 Optical Society of America

<http://dx.doi.org/10.1364/ao.XX.XXXXXX>

The measurement of wide-field two-dimensional time-integrated dynamic speckle patterns (2D-TIDSPs) for the purpose of blood flow measurement using inexpensive, low frame rate cameras, is a task that is performed in a variety of modalities in biomedical optics. The oldest example of this is laser speckle contrast imaging (LSCI), which was developed in the 1980s [1]. LSCI infers blood flow index (BFI) as $1/K^2$, where K is the speckle contrast of a 2D-TIDSP that has been backscattered from the sample [2]. A related technique, multi-exposure speckle imaging (MESI), is based on the acquisition of a series of 2D-TIDSPs using multiple camera exposure times [3].

Diffuse correlation spectroscopy (DCS) is a modality that is able to measure blood flow at greater imaging depths than LSCI and MESI through the recovery of the field autocorrelation function, $g_1(\tau)$. This technique is traditionally limited to single mode photon counting detection [4]; however, one group has recently demonstrated the feasibility of recovering equivalent information from multi-exposure 2D-TIDSPs through the use of the multi-step Volterra integral method (MVIM) [5]. Additionally, our group has presented a system which makes use of low frame rate camera-based detection in the Fourier domain to acquire DCS data using a heterodyne holographic detection technique [6, 7].

Diffuse speckle pulsatile flowmetry (DSPF) has recently been presented and is a technique that extends diffuse speckle contrast analysis (DSCA) from single mode to multimode detection, with a subsequent improvement in the measurement rate of deep

tissue blood flow that is equal to the camera frame rate [8]. Speckle contrast optical tomography (SCOT) reconstructs 3D maps of deep tissue blood flow by utilising information from all the source-detector pairs that are detected by an array of detectors, such as that present within a camera [9].

The motivation to simulate speckle patterns has previously been put forward by Song *et al.* [10], who explained that simulation techniques are a useful complement to experimental investigation with regard to understanding speckle phenomena and their practical application [11–13]. Simulation is also a useful tool for evaluating data processing methods [14, 15] and for investigating the feasibility of novel applications of laser speckle.

Two techniques have been described in the literature to model the evolution of a speckle pattern between two statistically independent fully-developed speckle patterns, based on the expected properties of $g_1(\tau)$. The first of these is the copula method [16], an empirical approach that was used [12, 14, 15] to simulate 2D-TIDSPs; however, the solutions offered by this technique do not model static scatterers and are restricted to only a few prescribed forms of $g_1(\tau)$. The second technique is a first principles approach [10] that allows for the generation of a series of fully developed speckle patterns with corresponding spatial variations in $g_1(\tau)$. This technique does not restrict the form of $g_1(\tau)$ that is used, and it is also able to model static scatterers. However, we have found that integrating over time in such an evolution does not simulate a 2D-TIDSP with statistically accurate speckle contrast, the property from which sample motion may be inferred. This is because this approach does not take into account the number of statistically independent degrees of freedom (or temporal coherence lengths), \mathcal{M} , that influence a time-integrated speckle measurement [17].

Goodman employed the concept of independent degrees of freedom to generate an approximate solution for the probability density function (PDF) of a 2D-TIDSP, and also described an approach to obtain an exact solution for this problem that makes use of the Karhunen-Loève expansion of the electric field [17]. In this letter we extend this latter approach and propose new insights to simulate 2D-TIDSP *images* in biomedical optics. By doing so we build a robust forward model for the simulation of 2D-TIDSPs that accounts for spatial variation in $g_1(\tau)$ (with known scatterer motion and decorrelation time), camera integration time, contributions from dynamic and static scatterers, and

the coherent transfer function (CTF) of the instrument.

We wish to evaluate the measured intensity of a 2D-TIDSP as

$$\mathbf{W} = \int_0^T \mathbf{U}(t) \mathbf{U}^*(t) dt, \quad (1)$$

where $\mathbf{U}(t)$, the complex valued field, is a random process that has autocorrelation function $g_1(\tau)$, where τ is the delay time $t_2 - t_1$, $g_1(\tau)$ measures the statistical similarity of $\mathbf{U}(t_1)$ and $\mathbf{U}(t_2)$ over a measured spatial ensemble, and we use bold notation to indicate a 2D xy dependency.

We note that $g_1(\tau)$ has contributions from both dynamic and static scatterers [18]

$$g_1(\tau) = \alpha |g_{1d}(\tau)| + (1 - \alpha), \quad (2)$$

where α is the fraction of the dynamic scattering component, and in this letter we consider

$$g_{1d}(\tau) = \exp\left(-\left(\frac{\tau}{\tau_c}\right)^p\right), \quad (3)$$

for values of $p = [0.5, 1, 2]$, where τ_c is the decorrelation time of the sample [2]. These three forms of $g_{1d}(\tau)$ can be used to model sample motion in LSCI experiments according to scattering regime (i.e., single or multiple), particle motion type (i.e., ordered or unordered) and approximate vessel size [2, 19, 20]. Values of $p = 1$ and $p = 2$ can also be used to model Brownian and convective motion in DCS experiments, respectively, under certain conditions [21].

With a view to calculating 2D-TIDSP PDFs, Goodman showed that $\mathbf{U}(t)$ can be expanded into an infinite series of statistically independent and uncorrelated modes [17]. Here we extend this approach to the simulation of 2D-TIDSP images for fully polarised light, by firstly considering the inverse Karhunen-Loève expansion of $\mathbf{U}(t)$ on the interval $(0, T)$ into a weighted sum of basis vectors

$$\mathbf{U}(t) = \sum_{n=1}^{\infty} \phi_n(t) \hat{\mathbf{U}}_n, \quad (4)$$

where $\phi_n(t)$ is a set of orthonormal and complete functions, such that

$$\int_0^T \phi_n(t) \phi_m^*(t) dt = \begin{cases} 1 & n = m \\ 0 & n \neq m, \end{cases} \quad (5)$$

and the expansion coefficients $\hat{\mathbf{U}}_n$ are uncorrelated modes given by $\hat{\mathbf{U}}_n = \int_0^T \phi_n^*(t) \mathbf{U}(t) dt$. By design, the Karhunen-Loève expansion maximally decorrelates the expansion coefficients $\hat{\mathbf{U}}_n$, and thus for a zero mean process we require that

$$E[\hat{\mathbf{U}}_n \hat{\mathbf{U}}_m^*] = \begin{cases} \lambda_n & n = m \\ 0 & n \neq m, \end{cases} \quad (6)$$

which can be achieved when the set $\{\phi_n(t)\}$ satisfies the integral equation $\int_0^T g_1(t_2 - t_1) \phi_n(t_1) dt_1 = \lambda_n \phi_n(t_2)$, i.e., $\phi_n(t)$ and λ_n are the set of eigenfunctions and eigenvalues, respectively, of the integral equation that has $g_1(\tau)$ as its kernel [22].

Substituting Eq. 4 into Eq. 1, we have

$$\mathbf{W} = \sum_{n=1}^{\infty} \sum_{m=1}^{\infty} \hat{\mathbf{U}}_n \hat{\mathbf{U}}_m^* \int_0^T \phi_n(t) \phi_m^*(t) dt, \quad (7)$$

which, using Eq. 5, simplifies to

$$\mathbf{W} = \sum_{n=1}^{\infty} \hat{\mathbf{U}}_n \hat{\mathbf{U}}_n^*, \quad (8)$$

and \mathbf{W} has been expressed as the sum of an infinite number of uncorrelated and statistically independent modes. Each $\hat{\mathbf{U}}_n \hat{\mathbf{U}}_n^*$ represents a statistically independent instantiation of the instantaneous intensity of fully polarised light, which adheres to negative exponential statistics and is statistically equivalent to a fully developed speckle pattern [17]. We therefore propose that the time integrated signal as a function of space (i.e., one 2D-TIDSP) may be simulated as the weighted sum of N uncorrelated and statistically independent fully developed 2D speckle patterns, each of which has a corresponding mean value of $E[\hat{\mathbf{U}}_n \hat{\mathbf{U}}_n^*] = \lambda_n$. We consider first the case of homogeneous fields (i.e., spatially invariant λ_n); however, we relax this assumption later in the letter when considering spatially heterogeneous fields.

The intensity of an instantiation of a fully developed speckle pattern follows negative exponential statistics, the weighted spatial sampling of which can be modelled by [10, 23]

$$\mathbf{I}_n = |\hat{\mathbf{U}}_n|^2, \quad (9)$$

where

$$\hat{\mathbf{U}}_n = F[\exp(-i\Omega_n)] \sqrt{\lambda_n} \quad (10)$$

is the corresponding field, where F denotes the 2D discrete Fourier transform and each Ω_n is an independent instantiation of uniformly distributed random variables in a 2D matrix on the interval $(-\pi, \pi)$. Incorporating the CTF of a coherent imaging system, Eq. 9 becomes [10, 16, 23]

$$\mathbf{I}_n = \left| F^{-1}[\hat{\mathbf{U}}_n \mathbf{H}] \right|^2, \quad (11)$$

where \mathbf{H} is the CTF. In this letter, we model 600 x 600 pixel images and all simulations model \mathbf{H} as a central circle function of diameter 200 pixels [10]; we therefore expect each modelled speckle to occupy a square region with a width of three pixels.

To compute the values of λ_n we adapt the routine described by Goodman [17, 23]. $g_1(\tau)$ (Eq. 2) is linearly discretised over the camera exposure period, T , by sampling the function $g_1(|t_2 - t_1|)$ over a 2D $N \times N$ matrix, for values of $t_1 = (0, T/(N-1), \dots, T)$ on one matrix axis, and for values of $t_2 = (0, T/(N-1), \dots, T)$ on the other matrix axis. λ_n are then the N eigenvalues of this $g_1(\tau)$ square sampling matrix, and in this letter we use a value of $N = 500$ for homogeneous field simulations. An example of this process is shown in Fig. 1 (whilst Fig. S1 of Supplement 1 demonstrates how the individual λ_n values vary as a function of T/τ_c). The exact nature of this solution becomes approximate due to this discretisation; however, we have found that using this value of N provides a

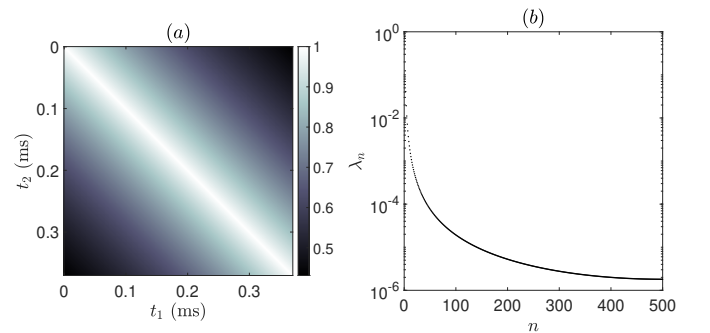


Fig. 1. (a) Sampling of $g_1(|t_2 - t_1|)$ for $T = 0.37$ ms, $\tau_c = 0.37$ ms, $\alpha = 0.9$, $p = 1$ and $N = 500$. (b) The N eigenvalues, λ_n , of the square matrix (a).

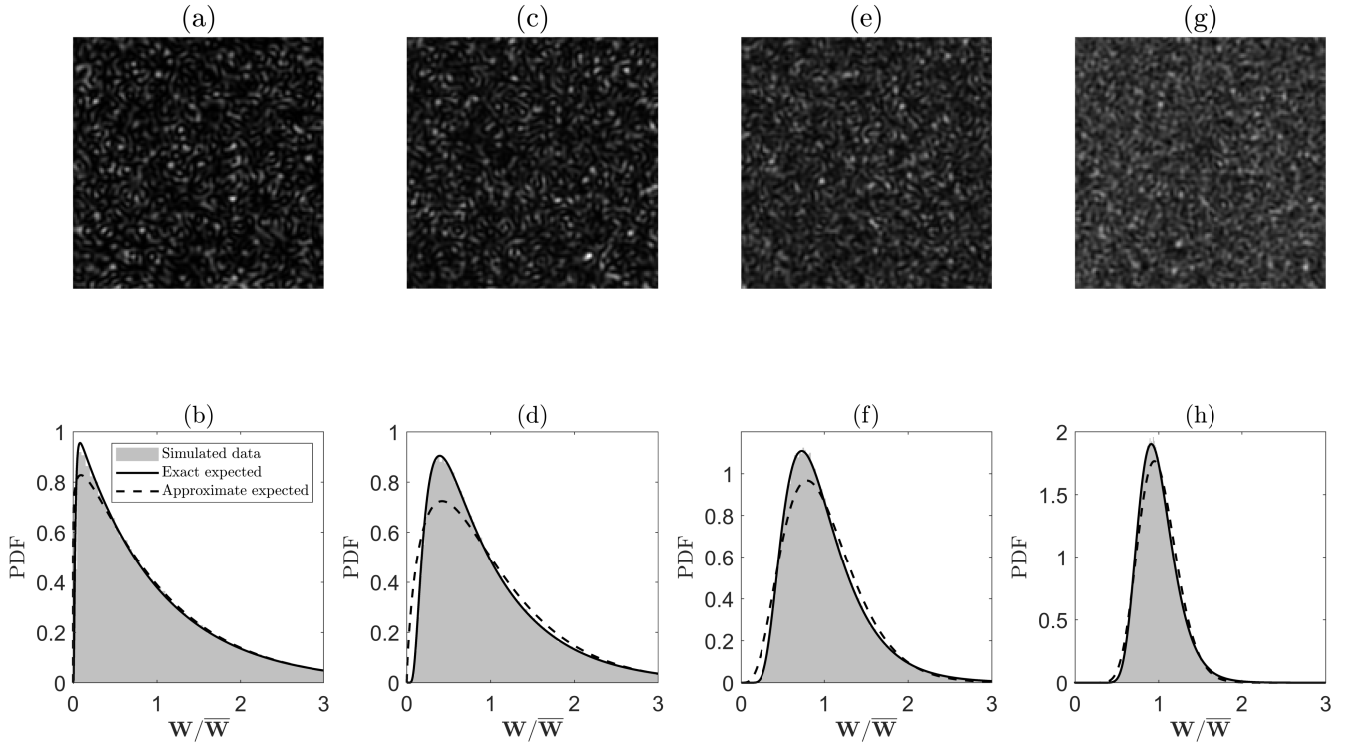


Fig. 2. Simulated 2D-TIDSPs and their corresponding image histograms for $p = 1$, $\alpha = 0.9$, $\tau_c = 0.37$ ms, (a-b) $T/\tau_c = 0.1$, (c-d) $T/\tau_c = 1.0$, (e-f) $T/\tau_c = 5.0$ and (g-h) $T/\tau_c = 25.0$. The top row shows a 150×150 pixel region of interest (ROI) of each 2D-TIDSP. Exact and approximate expected PDFs [17] are superimposed on the image histograms.

sufficient level of accuracy for the range of T/τ_c ratios used in our homogeneous field simulations. The impact of the choice of N on the computational performance of this algorithm, together with considerations on how to optimise performance, are given in Section S2 of Supplement 1.

For homogeneous field simulations we use a value of $\tau_c = 0.37$ ms [10], and simulated 2D-TIDSPs for such fields are shown in the top row of Fig. 2 for $p = 1$, $\alpha = 0.9$ and various camera integration times. The bottom row of this figure shows the corresponding image histograms of the mean normalised 2D-TIDSPs. In each case there is excellent agreement with Goodman's exact PDF solution [17], which serves to validate our simulation in terms of intra-image statistics. In this figure we also show Goodman's approximate PDF solution, which deviates from the simulated data, especially at intermediate values of T/τ_c .

We then sought to validate our simulation technique against analytical solutions for speckle contrast, which is defined as the ratio of standard deviation, σ , to mean intensity, μ , of a sample of speckles and can be related to $g_1(\tau)$ through [8, 19]

$$K = \frac{\sigma}{\mu} = \left[\frac{2\beta}{T} \int_0^T \left(1 - \frac{\tau}{T}\right) [g_1(\tau)]^2 d\tau \right]^{1/2}, \quad (12)$$

where β is the coherence factor. For the form of $g_{1d}(\tau)$ given by Eq. 3, the specific solutions to Eq. 12 (i.e., K_p for $p = [0.5, 1, 2]$) have recently been published [20]. We note that our simulation framework does not parameterise β , and considerations on the feasibility of this are included in Section S3 of Supplement 1.

We validated our simulation technique for different types of scatterer motion by simulating 2D-TIDSPs with homogeneous fields for $p = [0.5, 1, 2]$ and $\alpha = 0.9$ for the range of T/τ_c ratios shown in Fig. 3. The global speckle contrast of each 2D-TIDSP

was calculated, and (for each value of p) the resulting values of K_p were fit to the respective analytical solution to Eq. 12 by minimisation of the least squares objective function

$$\operatorname{argmin}_{(\tau_c, \beta, \alpha)} \sum_{i=1}^x [K_p(T_i)_{\text{simulated}} - K_p(T_i)_{\text{model}}]^2 \quad (13)$$

over x values of T . The resulting model fits and extracted parameter values shown in Fig. 3 are in excellent agreement with our simulation parameters and simulated data. We note that although we expect each speckle to occupy nine image pixels for this fully polarised model, this is not a perfect mapping and some pixels will have contributions from more than one speckle. The fitted values of β shown in Fig. 3 are therefore slightly less than 1.

We now consider the case of spatial variations in $g_1(\tau)$, which we treat by allowing λ_n to have a spatial dependence. This is done by partitioning the sample into labelled sub-domains, each having uniform $g_1(\tau)$ and, therefore, λ_n . We then evaluate Eq. 10 for each sub-domain, where the support of each \hat{U}_n is given by the corresponding sub-domain. We can model the smooth transition between adjacent tissue types by increasing the number of labels; however, the incorporation of the CTF into our simulation will also perform this smoothing function. Please see Section S2 of Supplement 1 for further details. To demonstrate this approach for a realistic yet arbitrary *in vivo* sample, we adapted with permission the *in vivo* optical-resolution photoacoustic microscopy (OR-PAM) image from Fig. 5(a) of [24], which shows an 8 mm \times 8 mm field of view of the microvasculature of a mouse ear. Using an approach similar to that demonstrated by Song *et al.* [10], we partitioned the image into five grayscale labels, as shown in Fig. 4(a), and assigned arbitrary

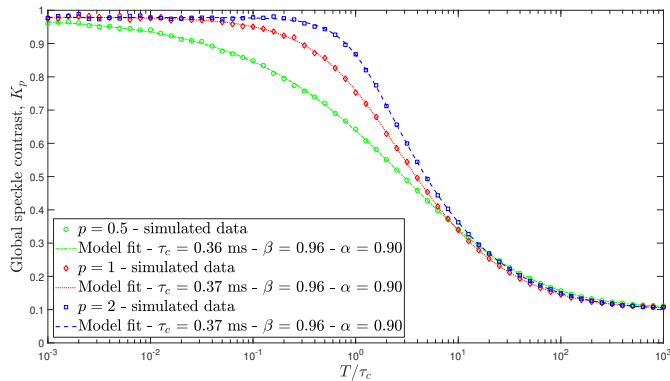


Fig. 3. Global speckle contrast values of simulated 2D-TIDSPs for $p = [0.5, 1, 2]$, $\alpha = 0.9$, $\tau_c = 0.37$ ms and variable ratios of T/τ_c . Model fits to analytical solutions to Eq. 12 and extracted parameter values are also shown.

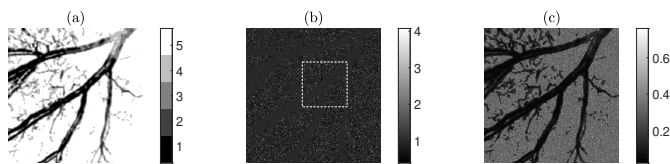


Fig. 4. (a) Partitioned OR-PAM image of mouse ear vasculature. (b) Example of one simulated 2D-TIDSP. A magnified view of the ROI within the white dashed square is shown in Fig. S2 of Supplement 1. (c) Temporal speckle contrast image computed from 30 simulated 2D-TIDSPs.

yet realistic values of τ_c in the range 0.05-1.0 ms [20] to each label. The image was sectioned to a 3.4 mm x 3.4 mm region of interest, and we assumed that areas of higher optical absorption in the OR-PAM image correspond to areas of higher flow. Thus values of $\tau_c = [0.05, 0.10, 0.20, 0.50, 1.00]$ ms were used, which corresponded to labels [1,2,3,4,5], respectively. Modelling values of $p = [1, 1, 1, 1, 0.5]$ and $\alpha = [1, 1, 1, 1, 0.8]$ for each label, we simulated 30 2D-TIDSPs using an exposure time of 20 ms [14]. By running the validation presented in Fig. 3, we find that a value of $N = 1000$ is necessary to ensure statistical accuracy for these simulation parameters. An example of a simulated 2D-TIDSP generated using the spatially varying λ_n for these specified simulation parameters is shown in Fig. 4(b). A temporal speckle contrast image was computed from this stack of 30 simulated 2D-TIDSPs, and this is shown in Fig. 4(c), where the speckle contrast values correspond well with the spatial distribution of τ_c . Considerations for the addition of measurement noise to simulated 2D-TIDSPs, as well as further validation of our algorithm using experimental techniques, are given in Section S4 of Supplement 1.

To the best of our knowledge, this letter represents the first time that a statistically robust algorithm for the simulation of 2D-TIDSPs, with specified temporal and spatial correlations, has been presented in the field of biomedical optics. Our proposed simulation technique is efficient and adaptable, and can readily be extended to include more complicated forms of $g_1(\tau)$ (such as that used to model the correlation diffusion equation in a semi-infinite geometry in DCS experiments [25], for example, which would also allow for the parameterisation of sample optical properties) and to accommodate mixed motion models, including those where the edges between different types of motion

are not sharp [2]. We therefore expect the technique presented here to be a powerful and useful simulation tool for the biomedical optics community for the purposes of understanding the practical application of speckle phenomena, evaluating data processing methods of speckle images, and assessing the feasibility of novel applications of laser speckle.

Funding. EPSRC-funded UCL Centre for Doctoral Training in Medical Imaging (EP/L016478/1); Engineering and Physical Sciences Research Council (EP/N032055/1); Royal Academy of Engineering Fellowship (RF1516\15\33); Royal Society (URF\R\191036, UF130304).

Acknowledgements. We thank James Guggenheim for providing the OR-PAM image that is used in this letter.

Disclosures. The authors declare no conflicts of interest.

Data availability. Data underlying the results presented in this paper are not publicly available at this time but may be obtained from the authors upon reasonable request.

Supplemental document. See Supplement 1 for supporting content.

REFERENCES

1. A. F. Fercher and J. D. Briers, *Opt. Commun.* **37**, 326 (1981).
2. D. D. Postnov, J. Tang, S. E. Erdener, K. Kiliç, and D. A. Boas, *Sci. Adv.* **6**, 1 (2020).
3. A. B. Parthasarathy, W. J. Tom, A. Gopal, X. Zhang, and A. K. Dunn, *Opt. Express* **16**, 1975 (2008).
4. T. Durduran and A. G. Yodh, *NeuroImage* **85**, 51 (2014).
5. K. Murali, A. K. Nandakumaran, T. Durduran, and H. M. Varma, *Biomed. Opt. Express* **10**, 5395 (2019).
6. E. James and S. Powell, *Biomed. Opt. Express* **11**, 6755 (2020).
7. E. James and S. Powell, *Proc. SPIE* **11239**, 29 (2020).
8. R. Bi, Y. Du, G. Singh, J.-H. Ho, S. Zhang, A. B. E. Attia, X. Li, and M. C. Olivo, *J. Biomed. Opt.* **25**, 1 (2020).
9. H. M. Varma, C. P. Valdes, A. K. Kristoffersen, J. P. Culver, and T. Durduran, *Biomed. Opt. Express* **5**, 1275 (2014).
10. L. Song, Z. Zhou, X. Wang, X. Zhao, and D. S. Elson, *Biomed. Opt. Express* **7**, 798 (2016).
11. S. J. Kirkpatrick, D. D. Duncan, and E. M. Wells-Gray, *Opt. Lett.* **33**, 2886 (2008).
12. O. B. Thompson and M. K. Andrews, *J. Biomed. Opt.* **15**, 1 (2010).
13. I. Fredriksson and M. Larsson, *J. Biomed. Opt.* **21**, 1 (2016).
14. J. Qiu, P. Li, W. Luo, J. Wang, H. Zhang, and Q. Luo, *J. Biomed. Opt.* **15**, 1 (2010).
15. H. Zhang, P. Li, N. Feng, J. Qiu, B. Li, W. Luo, and Q. Luo, *Opt. Express* **20**, 508 (2012).
16. D. D. Duncan and S. J. Kirkpatrick, *J. Opt. Soc. Am. A* **25**, 231 (2008).
17. J. Goodman, *Statistical Optics* (Wiley, Hoboken, New Jersey, 2015), 2nd ed.
18. D. A. Boas and A. G. Yodh, *J. Opt. Soc. Am. A* **14**, 192 (1997).
19. D. A. Boas and A. K. Dunn, *J. Biomed. Opt.* **15**, 1 (2010).
20. C. Liu, K. Kiliç, S. E. Erdener, D. A. Boas, and D. D. Postnov, *Biomed. Opt. Express* **12**, 3571 (2021).
21. E. J. Sie, H. Chen, E.-F. Saung, R. Catoen, T. Tiecke, M. A. Chevillet, and F. Marsili, *Neurophotonics* **7**, 1 (2020).
22. W. Davenport and W. Root, *Random Signals and Noise* (McGraw-Hill Book Company, New York, 1958).
23. J. Goodman, *Speckle Phenomena in Optics - Theory and Applications* (SPIE, Bellingham, Washington, 2020), 2nd ed.
24. J. A. Guggenheim, J. Li, T. J. Allen, R. J. Colchester, S. Noimark, O. Ogunlade, I. P. Parkin, I. Papakonstantinou, A. E. Desjardins, E. Z. Zhang, and P. C. Beard, *Nat. Photonics* **11**, 714 (2017).
25. T. Durduran, R. Choe, W. B. Baker, and A. G. Yodh, *Reports on Prog. Phys.* **73**, 076701 (2010).

FULL REFERENCES

1. A. F. Fercher and J. D. Briers, "Flow visualization by means of single-exposure speckle photography," *Opt. Commun.* **37**, 326–330 (1981).
2. D. D. Postnov, J. Tang, S. E. Erdener, K. Kiliç, and D. A. Boas, "Dynamic light scattering imaging," *Sci. Adv.* **6**, 1–9 (2020).
3. A. B. Parthasarathy, W. J. Tom, A. Gopal, X. Zhang, and A. K. Dunn, "Robust flow measurement with multi-exposure speckle imaging," *Opt. Express* **16**, 1975–1989 (2008).
4. T. Durduran and A. G. Yodh, "Diffuse correlation spectroscopy for non-invasive, micro-vascular cerebral blood flow measurement," *NeuroImage* **85**, 51–63 (2014).
5. K. Murali, A. K. Nandakumaran, T. Durduran, and H. M. Varma, "Recovery of the diffuse correlation spectroscopy data-type from speckle contrast measurements: towards low-cost, deep-tissue blood flow measurements," *Biomed. Opt. Express* **10**, 5395–5413 (2019).
6. E. James and S. Powell, "Fourier domain diffuse correlation spectroscopy with heterodyne holographic detection," *Biomed. Opt. Express* **11**, 6755–6779 (2020).
7. E. James and S. Powell, "Diffuse correlation spectroscopy in the Fourier domain with holographic camera-based detection," *Proc. SPIE* **11239**, 29–35 (2020).
8. R. Bi, Y. Du, G. Singh, J.-H. Ho, S. Zhang, A. B. E. Attia, X. Li, and M. C. Olivo, "Fast pulsatile blood flow measurement in deep tissue through a multimode detection fiber," *J. Biomed. Opt.* **25**, 1–10 (2020).
9. H. M. Varma, C. P. Valdes, A. K. Kristoffersen, J. P. Culver, and T. Durduran, "Speckle contrast optical tomography: A new method for deep tissue three-dimensional tomography of blood flow," *Biomed. Opt. Express* **5**, 1275–1289 (2014).
10. L. Song, Z. Zhou, X. Wang, X. Zhao, and D. S. Elson, "Simulation of speckle patterns with pre-defined correlation distributions," *Biomed. Opt. Express* **7**, 798–809 (2016).
11. S. J. Kirkpatrick, D. D. Duncan, and E. M. Wells-Gray, "Detrimental effects of speckle-pixel size matching in laser speckle contrast imaging," *Opt. Lett.* **33**, 2886–2888 (2008).
12. O. B. Thompson and M. K. Andrews, "Tissue perfusion measurements: multiple-exposure laser speckle analysis generates laser Doppler-like spectra," *J. Biomed. Opt.* **15**, 1–7 (2010).
13. I. Fredriksson and M. Larsson, "On the equivalence and differences between laser Doppler flowmetry and laser speckle contrast analysis," *J. Biomed. Opt.* **21**, 1–11 (2016).
14. J. Qiu, P. Li, W. Luo, J. Wang, H. Zhang, and Q. Luo, "Spatiotemporal laser speckle contrast analysis for blood flow imaging with maximized speckle contrast," *J. Biomed. Opt.* **15**, 1–5 (2010).
15. H. Zhang, P. Li, N. Feng, J. Qiu, B. Li, W. Luo, and Q. Luo, "Correcting the detrimental effects of nonuniform intensity distribution on fiber-transmitting laser speckle imaging of blood flow," *Opt. Express* **20**, 508–517 (2012).
16. D. D. Duncan and S. J. Kirkpatrick, "The copula: a tool for simulating speckle dynamics," *J. Opt. Soc. Am. A* **25**, 231–237 (2008).
17. J. Goodman, *Statistical Optics* (Wiley, Hoboken, New Jersey, 2015), 2nd ed.
18. D. A. Boas and A. G. Yodh, "Spatially varying dynamical properties of turbid media probed with diffusing temporal light correlation," *J. Opt. Soc. Am. A* **14**, 192–215 (1997).
19. D. A. Boas and A. K. Dunn, "Laser speckle contrast imaging in biomedical optics," *J. Biomed. Opt.* **15**, 1–12 (2010).
20. C. Liu, K. Kiliç, S. E. Erdener, D. A. Boas, and D. D. Postnov, "Choosing a model for laser speckle contrast imaging," *Biomed. Opt. Express* **12**, 3571–3583 (2021).
21. E. J. Sie, H. Chen, E.-F. Saung, R. Catoen, T. Tiecke, M. A. Chevillet, and F. Marsili, "High-sensitivity multispeckle diffuse correlation spectroscopy," *NeuroPhotonics* **7**, 1–15 (2020).
22. W. Davenport and W. Root, *Random Signals and Noise* (McGraw-Hill Book Company, New York, 1958).
23. J. Goodman, *Speckle Phenomena in Optics - Theory and Applications* (SPIE, Bellingham, Washington, 2020), 2nd ed.
24. J. A. Guggenheim, J. Li, T. J. Allen, R. J. Colchester, S. Noimark, O. Ogunlade, I. P. Parkin, I. Papakonstantinou, A. E. Desjardins, E. Z. Zhang, and P. C. Beard, "Ultrasensitive plano-concave optical microresonators for ultrasound sensing," *Nat. Photonics* **11**, 714–719 (2017).
25. T. Durduran, R. Choe, W. B. Baker, and A. G. Yodh, "Diffuse optics for tissue monitoring and tomography," *Reports on Prog. Phys.* **73**, 076701 (2010).